2020-08

Flow and magnetic structures in a kinematic ABC-dynamo

Zhang, T

10.1007/s11433-019-1568-x
Science China Physics, Mechanics & Astronomy
Springer Science and Business Media LLC

Supplementary materials: Flow and magnetic structures in a kinematic ABC-dynamo

Tao Zhang[1], Zhiliang Lin *[1,2], Chenyang Huang[1] and Alistair G. L. Borthwick[3]

[1]*State Key Laboratory of Ocean Engineering, School of Naval Architecture, Ocean and Civil Engineering, Shanghai Jiao Tong University, Shanghai 200240, China*

[2]*Collaborative Innovation Center for Advanced Ship and Deep-Sea Exploration, Shanghai 200240, China*

[3]*School of Engineering, The University of Edinburgh, Edinburgh EH9 3JL, United Kingdom*

S1 Brief introduction of Dynamo theory

The Earth's geomagnetic field helps deflect particles carried by the solar wind, and so protects the ozone layer. Since ancient times, people have been aware of the existence of an invisible field surrounding the Earth, as can be inferred from the invention of the compass from lodestone in the Han Dynasty (20BC-20AD). However, the mechanism behind the geomagnetic field has long puzzled scholars, the first insights being given by William Gilbert (1544-1603) who proposed that natural deposits of lodestone were responsible for the magnetic field. Later, Albert Einstein (1879-1955) proposed that the geomagnetic field could be caused by the asymmetric distribution of electron and proton charges on the Earth's surface, but this hypothesis was not accepted. In 1919, after observing the sunspot magnetic field, Joseph Larmor (1857-1942) conjectured that "it is possible for the internal cyclic motion to act after the manner of the cycle of a self-exciting dynamo, and maintain a permanent magnetic field from insignificant beginnings, at the expense of some of the energy of the internal circulation" [1]. Based on this concept, scientists have developed the so-called dynamo theory.

*Corresponding author: linzhiliang@sjtu.edu.cn.

Dynamo theory is used to explain the generation and maintenance of the magnetic field induced by a celestial body. The theory starts from the premise that electrically conductive fluid occupies the core of a given celestial body (an example being molten iron inside the Earth's outer core). This electrically conductive fluid undergoes rotational motion, being driven by thermal convection and Coriolis acceleration forces, and interacts with the initial weak magnetic field which is then continuously amplified [1]. This process is described in idealised form by the magnetic induction equation:

$$\frac{\partial \mathbf{B}}{\partial t} = \nabla \times (\mathbf{u} \times \mathbf{B}) + \eta \nabla^2 \mathbf{B} \tag{1}$$

where $\mathbf{B}$ is the magnetic field, $\mathbf{u}$ is the flow field of the conductive fluid, and η is the reciprocal of the magnetic Reynolds number and represents the magnetic diffusivity. The right-hand side comprises convection and diffusion terms, with corresponding (fast) convection and (slow) ohmic diffusion time scales. Dynamo theory initially proved problematic because its goal was to find a flow pattern that leads to a rapidly growing and stable solution of the magnetic field $\mathbf{B}$ in order to explain the generation and maintenance of the celestial magnetic field. However, the solution for most flow patterns evolved at the ohmic diffusion time scale, with the time required for exponential magnification for celestial bodies larger than a small star even greater than the age of the universe, giving rise to the so-called "slow dynamo"[2], which was obviously not realistic. A solution was needed that grew at the convective time scale, i.e. the so-called "fast dynamo".

S2 Finite time Lyapunov exponent (FTLE)

The concept of a Lagrangian coherent structure (LCS) was first proposed by Haller et al. [3] to describe the most repelling and attracting material surfaces that form the transport barriers in Lagrangian particle dynamics, and has since proved to be particularly useful in studies of chaotic flows. According to its original definition, LCS occupies ridges in the finite time Lyapunov exponent (FTLE) field. In practice, computation of the FTLE field provides a means by which to reveal otherwise hidden structures. Shadden et al. [4] give a detailed introduction to the FTLE. In short, FTLE is a finite time average of the maximum expansion rate obtained for a pair of particles advected by the flow. At first, it is necessary to define the flow map, which transfers tracer points from their position vector $\mathbf{x}_0 \in D$ at time t_0 to their new position vector $\mathbf{x} \in D$ at time t. The

flow map is denoted by $\phi_{t_0}^t$ and satisfies:

$$\phi_{t_0}^t : D \to D : \mathbf{x_0} \mapsto \phi_{t_0}^t(\mathbf{x_0}) = \mathbf{x}(t; t_0, \mathbf{x_0}), \tag{2}$$

$$\begin{cases} \phi_{t_0}^{t_0}(\mathbf{x}_0) &= \mathbf{x}_0 \\ \\ \phi_{t_0}^{t+s}(\mathbf{x}) &= \phi_s^{t+s}(\phi_{t_0}^s(\mathbf{x_0})) = \phi_t^{t+s}(\phi_{t_0}^t(\mathbf{x}_0)). \end{cases} \tag{3}$$

Without loss of generality, consider a tracer point located at $\mathbf{x} \in D$ at the time instant t_0. On advection, this tracer point moves to $\phi_{t_0}^{t_0+T}(\mathbf{x})$ over a time interval T. To assess the level of stretching of this trajectory, we consider the evolution of the perturbed point $\mathbf{y} = \mathbf{x} + \delta\mathbf{x}(0)$, where $\delta\mathbf{x}(0)$ is infinitesimal. For a time interval T, the perturbation becomes:

$$\delta\mathbf{x}(T) = \phi_{t_0}^{t_0+T}(\mathbf{y}) - \phi_{t_0}^{t_0+T}(\mathbf{x}) = \frac{\mathrm{d}\phi_{t_0}^{t_0+T}(\mathbf{x})}{\mathrm{d}\mathbf{x}}\delta\mathbf{x}(0) + \mathcal{O}(\|\delta\mathbf{x}(0)\|^2). \tag{4}$$

Growth of a linearized perturbation is determined by dropping the $\mathcal{O}(\|\delta\mathbf{x}(0)\|^2)$ terms, and using the standard spectral norm, to obtain the maximal magnitude of the perturbation as:

$$\max_{t_0<t<T} \|\delta\mathbf{x}(T)\| = \sqrt{\lambda_{max}(\Delta)}\|\overline{\delta\mathbf{x}}(0)\|. \tag{5}$$

Here, the symmetric positive matrix

$$\Delta = \left[\frac{\mathrm{d}\phi_{t_0}^{t_0+T}(\mathbf{x})}{\mathrm{d}\mathbf{x}}\right]^* \left[\frac{\mathrm{d}\phi_{t_0}^{t_0+T}(\mathbf{x})}{\mathrm{d}\mathbf{x}}\right] \tag{6}$$

is the Cauchy-Green (C–G) strain tensor, where the superscript $*$ denotes the matrix transpose. Supposing that the stretching is exponential, equation (6) becomes:

$$\max_{t_0<t<T} \|\delta\mathbf{x}(T)\| = e^{\sigma_{t_0}^T(\mathbf{x})|T|}\|\overline{\delta\mathbf{x}}(0)\| \tag{7}$$

where

$$\sigma_{t_0}^T(\mathbf{x}) = \frac{1}{|T|}\ln\sqrt{\lambda_{max}(\Delta)} \tag{8}$$

is the largest finite time Lyapunov exponent in the time interval T, representing the magnitude of stretching at the point $\mathbf{x}$. It should be noted that the aforementioned computation of FTLE is forward in time, and so the ridge of the field reveals the location where most stretching takes place, called the repelling structure. Conversely, computing the field backward in time enables the most attracting locations to be identified, the so-called attracting structure. Both the repelling and

attracting structures are Lagrangian coherent structures. Generally, in two-dimensional flow, both these structures are in the form of curves, whose intersections are stagnation points. However, in three-dimensional flow, the structures occupy curved surfaces, and so are much harder to discern compared to their two-dimensional counterparts.

The present paper proposes a new scheme for identifying intersections between repelling and attracting structures in 3-D flows. Let the forward FTLE field be E_f, the backward FTLE field be E_b, and the FTLE values corresponding to the repelling and attracting surface be E_r and E_a, respectively. Then, E_T is a new field defined as:

$$E_T = E_f + E_b. \tag{9}$$

Thus, the iso-surface with $E_T = E_r + E_a$ can be used to represent the intersections of repelling and attracting surfaces.

S3 Properties of fluid particles on the skeleton structures

Table S1 lists the locations of all stagnation points in the ABC-flow with $A = B = C = 1$. To examine the behaviour of particles on a typical skeleton structure, we consider the line connecting stagnation points S_2 and G_1, whose analytical expression is:

$$\begin{cases} y &= \frac{3}{4}\pi \\ z &= \frac{3}{2}\pi - x \end{cases} \tag{10}$$

Substituting Eq. (10) into Eq. (1), we obtain:

$$\mathbf{u} = (-\cos x - \frac{\sqrt{2}}{2},\ 0,\ \cos x + \frac{\sqrt{2}}{2}) \tag{11}$$

Obviously, the velocity of a fluid particle, lying on the skeleton structure expressed by Eq. (10), constrains the particle so that it can only move along the skeleton, i.e. along the line from S_2 to G_1. Using similar arguments, all the other skeleton structures can be shown to have the same property.

Dombre et al. [5] also analyzed the relation between the A, B, C parameters and the number of stagnation points. They found that 8 stagnation points exist within the cube $[0,\ 2\pi]^3$ when

Table S1. Locations of α-type (S_i) and β-type (G_i) stagnation points

No.	S_i	G_i
1	$(7\pi/4, 7\pi/4, 7\pi/4)$	$(3\pi/4, 3\pi/4, 3\pi/4)$
2	$(5\pi/4, 3\pi/4, 1\pi/4)$	$(\pi/4, 7\pi/4, 5\pi/4)$
3	$(\pi/4, 5\pi/4, 3\pi/4)$	$(5\pi/4, \pi/4, 7\pi/4)$
4	$(3\pi/4, \pi/4, 5\pi/4)$	$(7\pi/4, 5\pi/4, \pi/4)$

A^2, B^2 and C^2 form a triangle (i.e. satisfy $A^2 < B^2 + C^2$ $(A \geq B \geq C)$), 4 stagnation points exist at critical conditions when $A^2 = B^2 + C^2$; and otherwise no stagnation points exist. In the present work, we study the coherent structures in ABC-flow with $A = B = C = 1$, which has 8 stagnation points. It is intended that the other two situations will be examined in future research.

S4 Numerical simulation of the induced magnetic field

The kinematic dynamo problem involves the flow geometry without considering the effect of the self-generated magnetic field on the velocity field. The dynamo merely requires a flow geometry in which the current generated by the fluid flow across a seed magnetic field produces a new magnetic field that amplifies and reinforces the original seed field. If the flow field is steady, then the magnetic induction equation turns into a non-selfadjoint eigenvalue problem. The real parts of the eigenvalues are called growth rates, of which the maximum growth rate (MGR) represents the exponential growth rate of the magnetic energy. The imaginary part of the eigenvalue, corresponding to the maximum growth rate, is related to the turnover period of the magnetic field.

In this paper, the evolution of the magnetic field is governed by Eq. (1), and the velocity field $\mathbf{u}$ is the ABC-flow, taking the form:

$$\mathbf{u} = (A\sin z + C\cos y, B\sin x + A\cos z, C\sin y + B\cos x). \tag{12}$$

Following Galloway [6], we use a fully spectral method with explicit mode coupling, such that:

$$\mathbf{B} = \sum_{m}^{N}\sum_{n}^{N}\sum_{l}^{N} (X_{m,n,l},\, Y_{m,n,l},\, Z_{m,n,l})\, e^{i(mx+ny+lz)} \tag{13}$$

where m, n, and l represent modes in the x, y, and z directions, and N is the number of modes. Then the velocity $\mathbf{u}$ can be rewritten as:

$$\mathbf{u} = \left(A\frac{e^{iz} - e^{-iz}}{2i} + C\frac{e^{iy} + e^{-iy}}{2},\ B\frac{e^{ix} - e^{-ix}}{2i} + A\frac{e^{iz} + e^{-iz}}{2},\ C\frac{e^{iy} - e^{-iy}}{2i} + B\frac{e^{ix} + e^{-ix}}{2} \right). \quad (14)$$

Substituting Eqs. (13) and (14) into equation (1), we finally obtain:

$$\begin{aligned} \dot{X}_{m,n,l} = n \Bigg[& \frac{A}{2}(Y_{m,n,l-1} - Y_{m,n,l+1}) + \frac{iC}{2}(Y_{m,n-1,l} + Y_{m,n+1,l}) \\ & - \frac{B}{2}(X_{m-1,n,l} - X_{m+1,n,l}) - \frac{iA}{2}(X_{m,n,l-1} + X_{m,n,l+1}) \Bigg] \\ & - l \Bigg[\frac{C}{2}(X_{m,n-1,l} - X_{m,n+1,l}) + \frac{iB}{2}(X_{m-1,n,l} + X_{m+1,n,l}) \\ & - \frac{A}{2}(Z_{m,n,l-1} - Z_{m,n,l+1}) - \frac{iC}{2}(Z_{m,n-1,l} + Z_{m,n+1,l}) \Bigg] \\ & + R_m^{-1} \left[n(mY_{m,n,l} - nX_{m,n,l}) - l(lX_{m,n,l} - mZ_{m,n,l}) \right] \end{aligned} \quad (15)$$

in the x direction. Equations for $Y_{m,n,l}$ and $Z_{m,n,l}$ are derived in the same way as above, and are not included here for brevity. Time integration is undertaken by the following Leapfrog scheme stabilised by a Dufort-Frankel discretization of the diffusive term:

$$\frac{X_{m,n,l}^{k+1} - X_{m,n,l}^{k-1}}{2\Delta t} = (C_t)_{m,n,l}^{k} - \frac{1}{2R_m}(m^2 + n^2 + l^2)\left(X_{m,n,l}^{k+1} + X_{m,n,l}^{k-1} \right) \quad (16)$$

where C_t is a convolution term. For the seed magnetic field (initial condition), we choose:

$$\mathbf{B}(t = 0) = (\cos z - \cos y,\ \cos x - \cos z,\ \cos y - \cos x) \quad (17)$$

to ensure the magnetic field is non-divergent. Based on the above procedure, the magnetic field induced by the ABC-flow is calculated. Then, the MGR and turnover period are obtained directly from the mode with largest magnetic energy. It is first necessary to verify convergence of the calculations. Taking $R_m = 16$ as an example (see Table S2), with a fixed time interval ($\mathrm{d}t = 0.01$), the maximum growth rate and turnover period of the magnetic field tend to be stable as the number of modes N increases. In the present work, the time interval $\mathrm{d}t$ has been carefully selected to ensure convergence of all numerical results.

The accuracy of all the numerical simulations is verified by comparison with previous results obtained by Galloway and Frisch [6], listed in Table S3. It can be seen that the present predictions of maximum growth rate and turnover period are reasonably consistent with those of Galloway

Table S2. Maximum growth rate (MGR) and turnover period, as a function of number of modes N, for the case $A = B = C = 1$.

N	MGR	Period
8	0.0132	10.7546
10	8.28E-04	10.522
12	0.0021	10.5983
14	0.0028	10.5907
16	0.0029	10.5918
18	0.0029	10.5918
20	0.0029	10.5918

Table S3. Maximum growth rate (MGR) and turnover period, as a function of the magnetic Reynolds number R_m, together with results obtained by Galloway and Frisch [6], for the case $A = B = C = 1$.

R_m	MGR (Present paper)	MGR ([3])	Period (Present paper)	Period ([3])
8	-0.0082	-0.0076	10.0112	10
10	0.0054	0.0053	10.0501	10
16	0.0029	0.0009	10.5918	10.5
24	-0.0057	-0.023	11.6557	11.4
27	0.0047	+small	49.2897	49
30	0.0129	0.013	50.8939	50.6
50	0.041	0.04	64.5117	64.5
60	0.0471	0.047	71.9482	72
70	0.0512	0.051	79.6474	80
100	0.0561	0.057	105.355	108
120	0.0566	0.059	126.2509	122

and Frisch. The largest discrepancies in growth rate between the present results and those of Galloway and Frisch occur when the magnetic Reynolds number is in the range from 16 to 27. The discrepancies mainly arise because insufficient modes were considered by Galloway and Frisch. For example, when $R_m = 16$ (see Table S2) and the mode number N equals 10, the present results are almost the same as those of Galloway and Frisch. Further confirmation is provided by the close agreement between the present predictions of growth rates with corresponding results obtained by Bouya [7]. Moreover, Table S3 shows that the turnover period jumps by a factor of about 4 when the magnetic Reynolds number increases from 24 to 27, in accordance with findings by Bouya [7].

S5 Evolution of the magnetic field

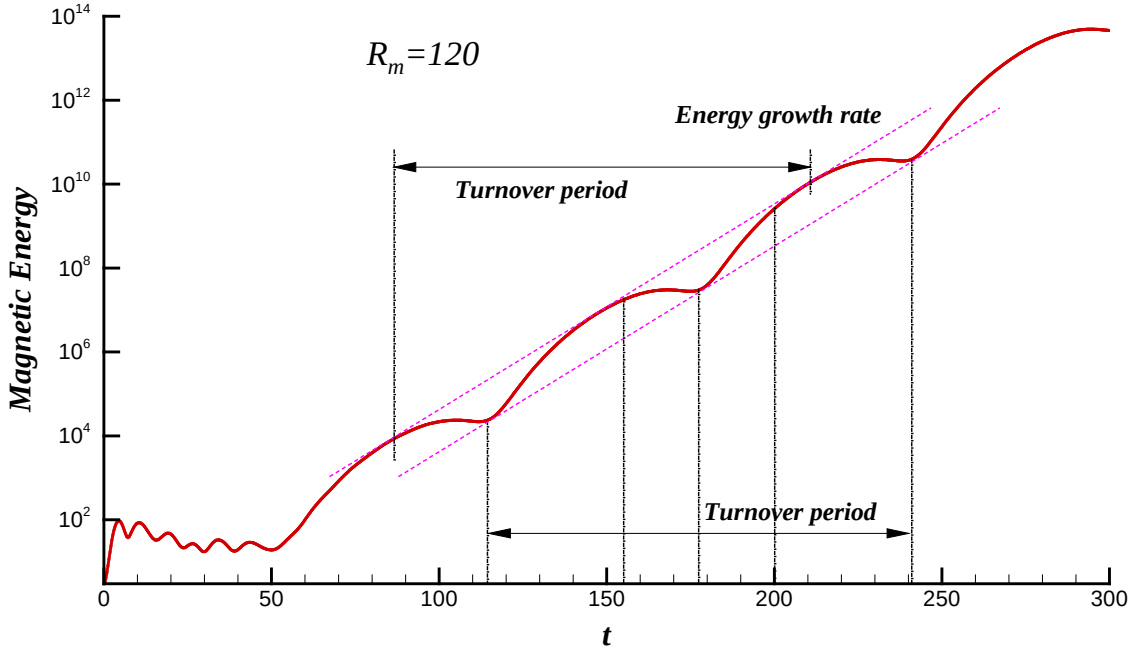

Fig. S1. Evolution of magnetic energy with time for $R_m = 120$ and $A = B = C = 1$. The turnover period of the magnetic field is 126.2509 and $MGR = 0.0566$. The blue dots a, b and c represent three different time instants, considered in the description of the magnetic structures.

In the numerical simulation of the magnetic field, the magnetic Reynolds number is set as $R_m = 120$, in which case the growth rate of the magnetic field is in a state of steady growth. The number of modes N in each direction in spectral space is 64, the time step dt is 0.005, and the resolution is fixed at $200 \times 200 \times 200$ for the transformation between spectral and physical space.

Figure S1 shows the time history of the total energy of the magnetic field. It can be seen that the energy of the magnetic field generally exhibits exponential growth with superimposed oscillation. The growth rate (two times of the MGR) of the magnetic energy and the turnover period are readily obtained from the curve. The magnetic fields at time instants $a\,(t = 155)$, $b\,(t = 177.5)$ and $c\,(t = 200)$ (denoted by blue dots) are considered representative and magnetic structures are explored to explain the turnover phenomenon in the letter.

S6 Location of the principal magnetic structure

The principal MS is the core structure of the magnetic field, which means that the principal MS plays a significant role in the evolution of the magnetic field. A question remains as to whether the principal MS can move to the location of one of the other three cigar-like structures, or elsewhere. Given that we do not consider the effect of different flow fields, the only possible factors that may change the magnetic field structures are the magnetic Reynolds number R_m and the initial magnetic distribution. Figure S2 shows the distribution of the principal MS obtained for three different initial conditions by replacing x, y, z in Eq. (17) with $x+\pi$, $y+\pi$, and $z+\pi$ respectively It is found that the principal MS can indeed be relocated by changing the initial distribution of the magnetic field.

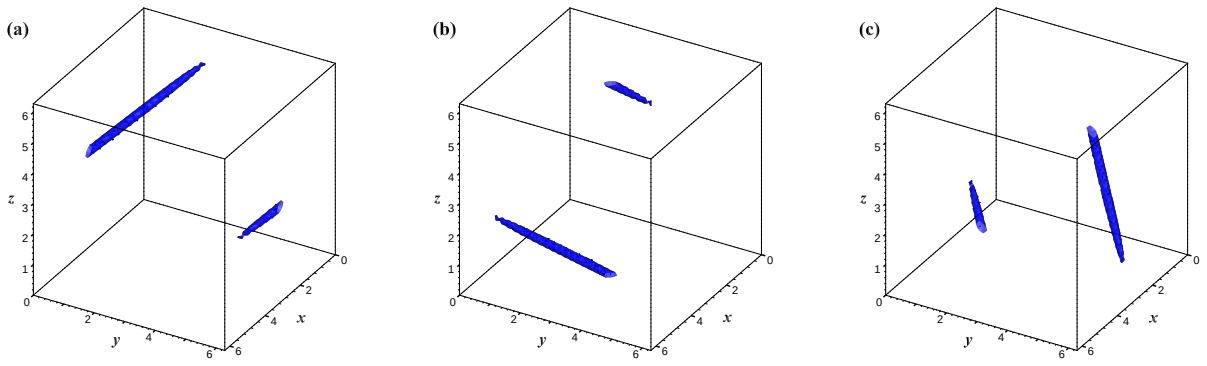

Fig. S2. Principal magnetic structures obtained using different seed magnetic fields, and denoted by iso-surfaces with $ME = 0.3ME_{max}$, for modified versions of Eq. (17): (a) replacing x with $x + \pi$; (b) replacing y with $y + \pi$; and (c) replacing z with $z + \pi$.

S7 Brief proof of perpendicular relation

As shown in Figure 3 of our letter, the axis of principal MS passes through S_1, whose coordinates are ($7\pi/4$, $7\pi/4$, $7\pi/4$). The direction vectors of the three lines (G_1S_2, G_1S_3 and G_1S_4) are (-1,1,0), (0,-1,1) and (1,0,-1), respectively. Thus, the normal vector of the plane $S_2S_3S_4$ is (1,1,1), which is exactly the same as the direction vector corresponding to the diagonal of the cube on which the principal MS lies.

References

[1] J.Larmor, 1919. "How could a rotating body such as the Sun become a magnet". Rep. Brit. Adv. Sci., pp. 159-160.

[2] D. Galloway, 2012. "ABC flows then and now". Geophys.Astrophys.Fluid Dyn., **106**(4-5), pp. 450–467.

[3] G. Haller, and G. C. Yuan, 2000. "Lagrangian coherent structures and mixing in two-dimensional turbulence". Physica D., **147**(3-4), pp. 352–370.

[4] S. C. Shadden, F. Lekien and J. E. Marsden, 2005. "Definition and properties of Lagrangian coherent structures from finite-time Lyapunov exponents in two-dimensional aperiodic flows". Physica D., **212**(3-4), pp. 271–304.

[5] T. Dombre, U. Frisch, J. M. Greene, M. Hénon, A. Mehr, and A. M. Soward, 1986. "Chaotic streamlines in the ABC flows". J. Fluid Mech., **167**, pp. 353–391 .

[6] D. Galloway, and U. Frisch, 1986. "Dynamo action in a family of flows with chaotic streamlines". Geophys.Astrophys.Fluid Dyn., **36**(1), pp. 53–83.

[7] I. Bouya, and E. Dormy, 2013. "Revisiting the ABC flow dynamo". Phys. Fluids., **25**(3), pp. 037103.